JACS
JOURNAL OF THE AMERICAN CHEMICAL SOCIETY

Communication

pubs.acs.org/JACS

Diffusion of CO_2 in Large Crystals of Cu-BTC MOF

Trenton M. Tovar,[†,∥] Junjie Zhao,[‡,∥] William T. Nunn,[‡] Heather F. Barton,[‡] Gregory W. Peterson,[§] Gregory N. Parsons,*[,‡] and M. Douglas LeVan*[,†]

[†]Department of Chemical and Biomolecular Engineering, Vanderbilt University, Nashville, Tennessee 37235, United States

[‡]Department of Chemical and Biomolecular Engineering, North Carolina State University, Raleigh, North Carolina 27695, United States

[§]Edgewood Chemical Biological Center, U.S. Army, Aberdeen Proving Ground, Maryland 21010, United States

Supporting Information

ABSTRACT: Carbon dioxide adsorption in metal−organic frameworks has been widely studied for applications in carbon capture and sequestration. A critical component that has been largely overlooked is the measurement of diffusion rates. This paper describes a new reproducible procedure to synthesize millimeter-scale Cu-BTC single crystals using concentrated reactants and an acetic acid modulator. Microscopic images, X-ray diffraction patterns, Brunauer−Emmett−Teller surface areas, and thermogravimetric analysis results all confirm the high quality of these Cu-BTC single crystals. The large crystal size aids in the accurate measurement of micropore diffusion coefficients. Concentration-swing frequency response performed at varying gas-phase concentrations gives diffusion coefficients that show very little dependence on the loading up to pressures of 0.1 bar. The measured micropore diffusion coefficient for CO_2 in Cu-BTC is 1.7×10^{-9} m^2/s.

The continuously increasing amount of CO_2 emissions due to anthropogenic activities has caused a sharp rise of CO_2 levels in the atmosphere.[1] While the search for alternative clean energy sources continues, developing new technologies for CO_2 capture and sequestration is still necessary and has significant impact for controlling global warming. Metal−organic frameworks (MOFs) are highly porous crystalline networks containing metal clusters interconnected by organic linkers.[2] MOFs typically have high surface areas that exceed those of traditional adsorbent materials.[3−7] In addition, the numerous options for the metal centers and linkers enable the rational design and synthesis of MOF structures to achieve enhanced adsorption capacities and catalytic properties. For example, MOFs have shown promising performance for CO_2/N_2 separation for postcombustion CO_2 removal from flue gas, CO_2/H_2 separation for precombustion capture, CO_2/CH_4 separation for natural gas upgrading, and direct capture of CO_2 from air.[1,8,9] MOFs also show excellent catalytic activities for converting CO_2 to valuable compounds.[10−13] As a result, MOFs are promising candidates for CO_2 capture and sequestration.

Despite the amount of research on CO_2 adsorption and separations and catalysis using MOFs, a major deficiency in the literature is the measurement of diffusion rates, a critical property that can significantly affect the overall performance for the above-mentioned applications. CO_2 diffusion constants have been reported for a few MOFs. Salles et al.[14] measured diffusion rates ranging from 10^{-8} to 10^{-9} m^2/s over a range of loadings on MIL-47(V). Sabouni et al.[15] reported a value of 7×10^{-12} m^2/s at 298 K for CPM-5, and Saha et al.[16] reported diffusion constants on the order of 10^{-9} m^2/s for MOF-177. Even for the same MOF (MOF-5), the reported diffusion coefficients show a wide range from 10^{-9} to 10^{-8} m^2/s.[16,17]

A big challenge for obtaining accurate diffusion coefficients is to decouple the presence of different mass transfer mechanisms related to the adsorbent morphology. For example, the impact of surface barriers on MOF thin films was explored by Heinke et al.[18] Fletcher et al.[19] found a linear driving force behavior for CO_2 in $Ni_2(4,4'\text{-bipy})_3(NO_3)_4$, but macropore diffusion was determined to be the controlling resistance for Co/DOBDC and Ni/DOBDC pellets by Hu et al.[20] using zero-length column techniques and for Cu-BTC pellets by Liu et al.[21] using concentration-swing frequency response (CSFR).

In this paper, we report a novel method to measure CO_2 micropore diffusion coefficients by using CSFR to analyze millimeter-scale MOF crystals. While large crystals have previously been used to aid diffusion measurements in zeolites,[22] this is the first such example for MOFs. We use Cu-BTC (HKUST-1) as a model to demonstrate this approach, as it shows one of the highest CO_2 capacities (under hydrated conditions) among all MOFs.[9] High selectivity for CO_2/H_2 and CO_2/N_2 separations have also been reported for this MOF.[23−26]

We developed a new synthesis technique to achieve millimeter-scale Cu-BTC single crystals, and the crystal size can be controlled well. A solution of $Cu(NO_3)_2{\cdot}3H_2O$ (0.49 g) and trimesic acid (H_3BTC) (0.24 g) in 9 mL of 1:1:1 (v/v/v) water/ethanol/DMF was mixed with 12 mL of glacial acetic acid (modulator), and the mixture was heated at 55 °C for 3 days. As aspects such as solvent residue and crystal defects can affect the diffusion rate, we carefully selected the crystals after the solvothermal synthesis and fully activated the MOFs (the detailed procedure is given in the Supporting Information).

Figure 1c−f shows optical micrographs and scanning electron microscopy (SEM) images of the Cu-BTC single crystals. Truncated cube and truncated octahedron shapes were observed for this *fcu*-type MOF crystal. The octagon (or square) facets represent the planes viewed down the ⟨100⟩ directions, while the

Received: June 9, 2016
Published: August 24, 2016

DOI: 10.1021/jacs.6b05930
J. Am. Chem. Soc. 2016, 138, 11449−11452

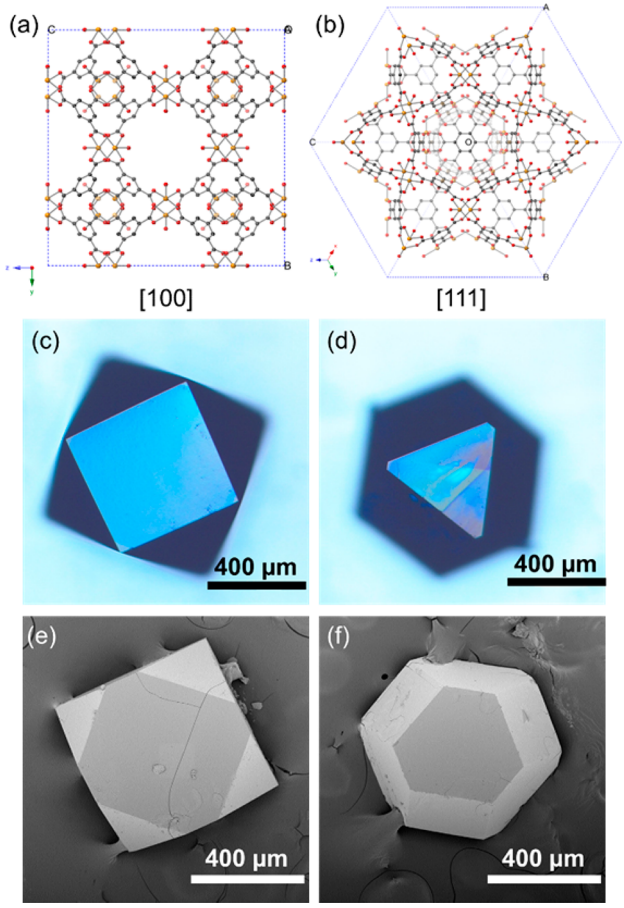

Figure 1. (a, b) Molecular representation of the Cu-BTC MOF along the [100] direction and [111] direction. Color code: Cu (yellow); O (red); C (black); H (not shown). (c, d) Optical microscopy and (e, f) SEM images of Cu-BTC single crystals.

hexagon-shaped facets correspond to the planes along the ⟨111⟩ directions. The sizes of Cu-BTC crystals obtained from 3-day syntheses range from 500 μm to 1.3 mm (Figure S2). These crystals were sorted by size for later CO_2 diffusion studies.

The quality of the Cu-BTC single crystals was characterized using X-ray diffraction (XRD), Brunauer–Emmett–Teller (BET) analysis, and thermogravimetric analysis (TGA). The XRD peak positions for the crystal planes parallel to (100) and (111) match well with the corresponding peaks present in the simulated diffraction pattern for Cu-BTC. The unit cell dimension (a = 26.35 Å) refined from single-crystal XRD measurements also agrees with the known value from the literature.[27]

The BET surface area (1980 m^2/g) and pore volume (0.85 cm^3/g) for the Cu-BTC single crystals are comparable to those of a Cu-BTC fine powder prepared from 85 °C solvothermal synthesis (Figure S4) and agree well with values from the literature.[23] The decomposition temperature regime of the large Cu-BTC crystals (300–385 °C) measured by TGA (Figure S5) is also similar to reported values.[28,29] These results all indicate the good quality of these MOF crystals. While previous work reported the use of nitric acid to inhibit the deprotonation of H_3BTC linker and thus reduce the crystal growth rate in order to achieve large single crystals,[30] our method using high concentrations of the MOF reactants and an acetic acid modulator is more effective and reproducible. The formation of an acetate complex competes with the generation of secondary building units in the solution, allowing the slow and steady growth of our single crystals. By avoiding high acidity of the precursor solution, we also obtained high crystal quality as shown above. In addition, the crystal size can be controlled well by varying the synthesis time (Figure S7).

Figure 2 compares the CSFR curves for a sample of large Cu-BTC single crystals and the powder at a gas-phase concentration

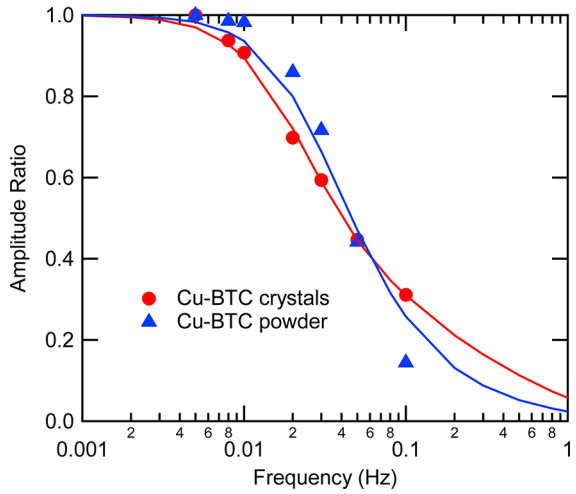

Figure 2. Amplitude ratio curves for CSFR experiments on large Cu-BTC crystals and a powder sample.

of 0.5% CO_2 and a total pressure of 1 bar. The CSFR curve for the Cu-BTC powder has a steeper slope than that for the single crystals, indicating faster CO_2 uptake in the powder. This is reasonable because the diffusion length in the powder (crystal size ~10 μm) is much shorter than for the millimeter-scale single crystals. We used an isothermal micropore diffusion model reported previously[31] to fit the curves and found that this model describes the single crystals well but shows noticeable deviation from the powder data. The micropore diffusion model fails to fit the powder data well because other diffusive mechanisms, such as surface barriers or external mass transfer, may also be involved in addition to micropore diffusion. For the millimeter-scale Cu-BTC single crystals, micropore diffusion is the dominant factor limiting the mass transfer rate, ensuring that the measured diffusion coefficients truly represent the diffusion inside the MOF micropores. While heat of adsorption effects can impact diffusion measurements, the CSFR apparatus can mitigate these effects.[32]

The isothermal micropore diffusion model uses two parameters to fit the CSFR curves; the regressed values are the local isotherm slope, K, and the micropore diffusion parameter D_s/R^2, where R is the diffusion length scale. As the regressed diffusion coefficient is dependent on the particle size, accurate diffusion measurements require precise knowledge of the crystal size, which is well-controlled by the synthesis technique. Three batches of Cu-BTC crystals with particle sizes of 0.7 ± 0.1 mm, 1.0 ± 0.1 mm, and 1.3 ± 0.1 mm were prepared, where the particle size corresponds to the longest crystal dimension. Each batch was used for CSFR measurements at 0.5% CO_2 concentration. Figure 3 shows the CSFR curves for each set of crystals, and the fitted parameters for the micropore diffusion model are given in Table 1. The regressed isotherm slopes show good agreement among the different crystal sizes, and D_s/R^2 decreases as the crystal size increases, as expected.

The micropore diffusion coefficients were calculated by multiplying the regressed diffusion parameter by the square of

DOI: 10.1021/jacs.6b05930
J. Am. Chem. Soc. 2016, 138, 11449–11452

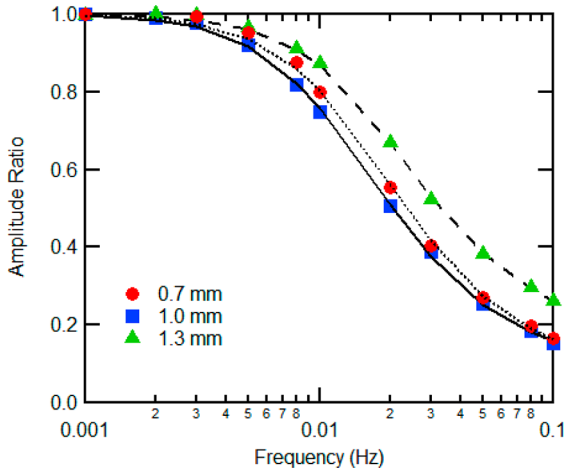

Figure 3. CSFR curves for different Cu-BTC crystal sizes at 0.5% CO_2 concentration.

Table 1. Micropore Diffusion Fitting Parameters for Various Cu-BTC Crystal Sizes at 0.5% CO_2

crystal size (mm)	K (mol kg^{-1} bar^{-1})	D_s/R^2 (s^{-1})	D_s (mm^2/s)
0.7	7.1	0.0110 ± 0.0012	0.0014 ± 0.0003
1.0	7.1	0.0082 ± 0.0009	0.0017 ± 0.0003
1.3	6.6	0.0066 ± 0.0005	0.0020 ± 0.0002

the diffusion length scale. However, the model assumes a spherical particle shape, which does not accurately represent the crystals. We found that the height of the crystals is approximately half of the longest dimension (L), indicating that the effective diffusion length should be smaller than L. We measured the average mass per crystal and correlated it as a function of L (Figure S6). A power law fit the data well with an exponent of 2.14 instead of the expected cubic function for a perfect sphere. To account for the shape factor, an effective diffusion length (R_{eff}) was defined as

$$\text{mass} = \rho\frac{4}{3}\pi {R_{eff}}^3 = \alpha {L_{meas}}^{2.14} \quad (1)$$

where L_{meas} (in units of mm) is the length of the longest crystal dimension, ρ (in units of g/cm^3) is the crystal density, and α = 0.52 mg/mm$^{2.14}$. For single crystals, the measured density is 1.29 g/cm^3, similar to reported values for Cu-BTC.[1,10] When normalized by R_{eff}, the micropore diffusion coefficients agree within experimental error and give an average value of 0.0017 mm^2/s (or 1.7 × 10^{-9} m^2/s). This value is on the same order of magnitude as several other CO_2 diffusion rates reported for other MOFs.

An important aspect of diffusion in nanoporous materials is the impact of the surface concentration on the diffusivity. Figure 4 shows the CSFR curves measured at various gas-phase concentrations using 18 mg of Cu-BTC single crystals with diameters of ∼0.7 mm. The steady-state CO_2 concentrations used in this series of experiments were 0.1%, 0.5%, and 10%. We found that the micropore diffusion model accurately fits the data at each tested CO_2 concentration. The curves are nearly identical for the 0.1% and 0.5% experiments, while the 10% curve is shifted to higher amplitude ratios, indicating a decrease in the local isotherm slope.

Table 2 summarizes the fitted parameters for the CSFR curves at each concentration as well as for a similar set of experiments on

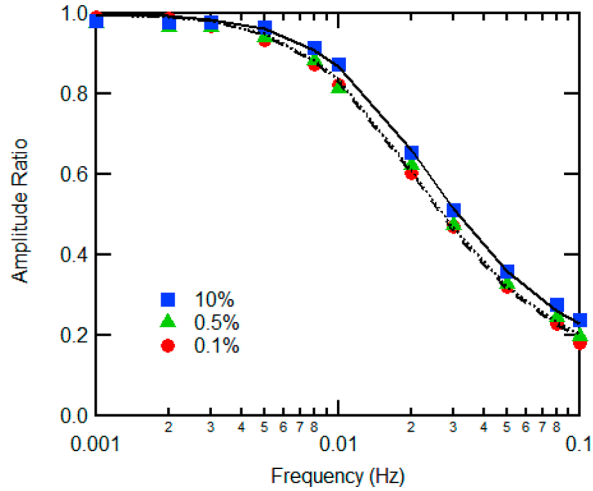

Figure 4. CSFR curves for various CO_2 concentrations on Cu-BTC crystals of approximately 1.5 mm.

BPL activated carbon (Figure S9), a predominantly microporous material that follows the micropore diffusion model well for various adsorbates.[33] For comparison, we also calculated the K values from the Toth fit of a CO_2 isotherm for the Cu-BTC crystals (Figure S10) and listed them in Table 2. The K values measured from CSFR experiments are slightly higher than those from the CO_2 isotherm, but the trends are very similar. For the 0.1% and 0.5% experiments, the isotherm slopes are similar, which agrees with the nearly linear shape of the CO_2 isotherm at such low concentrations. For the 10% experiment, the K value significantly decreases for both the CSFR and adsorption isotherm measurements.

It is very interesting that the diffusion coefficients for Cu-BTC single crystals and BPL activated carbon particles show completely different trends. For the single-crystal Cu-BTC samples, there is no significant difference in tests using CO_2 concentrations from 0.1% to 10%. However, for BPL activated carbon, the diffusion coefficient increases dramatically as a function of CO_2 concentration. These different trends are reasonable since the Cu-BTC single crystals have a narrow distribution of pore sizes, an ordered lattice structure, and therefore more homogeneous adsorption sites. At low pressure, CO_2 preferentially adsorbs at coordinatively unsaturated Cu sites.[34] After normalization of the CO_2 isotherm by the number of sites in the Cu-BTC structure, a per-site loading shows that all of the CSFR experiments were performed at pressures where there is less than one CO_2 molecule adsorbed per site. Thus, the adsorbate−adsorbent interaction remains similar as the CO_2 concentration increases. This also agrees well with experiments in the literature, as Wang et al.[35] reported that the heat of adsorption of CO_2 remains virtually constant as the loading increases after an initial decrease. In contrast, the BPL activated carbon is very heterogeneous, so the first CO_2 molecules will associate with stronger adsorption sites and will diffuse more slowly than at higher pressures.

In comparison with the MOF, the BPL activated carbon particles were larger (∼2 mm in diameter). After normalization by the diffusion length scale, the diffusion coefficient for the single MOF crystals is significantly lower than that for the activated carbon. This could be due to strong intermolecular interactions between CO_2 and the open metal sites of Cu-BTC. It could also be due to the small, ordered pore structures of Cu-BTC, whereas the activated carbon has a wide distribution of pore sizes.

DOI: 10.1021/jacs.6b05930
J. Am. Chem. Soc. 2016, 138, 11449−11452

Table 2. Micropore Diffusion Fitting Parameters for 0.7 mm Cu-BTC Single Crystals and BPL Activated Carbon at Different CO_2 Concentrations; Isotherm Slopes and CO_2 Uptakes Are Also Given

	Cu-BTC CSFR		BPL CSFR		Cu-BTC isotherm	
conc. (%)	K (mol kg^{-1} bar^{-1})	D_s/R^2 (s^{-1})	K (mol kg^{-1} bar^{-1})	D_s/R^2 (s^{-1})	K (mol kg^{-1} bar^{-1})	n_{CO_2}/site
0.1	6.9	0.0090	4.9	0.0024	5.9	0.0024
0.5	6.7	0.0086	4.2	0.0072	5.8	0.012
10	5.8	0.0089	2.8	0.0142	5.1	0.22

In conclusion, a new synthesis procedure to produce large millimeter-size single crystals of Cu-BTC has been reported. The crystal size could be accurately controlled by varying the synthesis time. Properties measured by XRD, BET analysis, TGA, and CO_2 isotherms on the Cu-BTC crystals agree well with those of Cu-BTC powders produced by traditional solvothermal synthesis. The increased length scale of the microporous domain makes diffusion measurements easier as it limits the impact of multiple mass transfer mechanisms. CSFR experiments verified micropore diffusion as the rate-controlling diffusive mechanism. Diffusion coefficients measured at varying concentrations showed very little dependence on the loading up to about 0.1 bar, the highest pressure considered. At 0.5% gas-phase concentration of CO_2 in He at 1 bar, the measured diffusion coefficient is approximately 1.7×10^{-9} m^2/s.

■ ASSOCIATED CONTENT

Supporting Information

The Supporting Information is available free of charge on the ACS Publications website at DOI: 10.1021/jacs.6b05930.

Procedures and additional data (PDF)

■ AUTHOR INFORMATION

Corresponding Authors

*gnp@ncsu.edu

*m.douglas.levan@vanderbilt.edu

Author Contributions

‖T.M.T. and J.Z. contributed equally.

Notes

The authors declare no competing financial interest.

■ ACKNOWLEDGMENTS

The authors acknowledge funding from ECBC (Grants W911SR-07-C-0075 and W911SR-13-0014) and the Joint Science and Technology Office (Army Research Office Grant W911NF-13-1-0173). J.Z. acknowledges Roger Sommer, Edward Sachet, and Prof. Jon-Paul Maria for the XRD measurement of single crystals and appreciates the use of the thermogravimetric analyzer in Prof. Saad Khan's group.

■ REFERENCES

(1) Sumida, K.; Rogow, D. L.; Mason, J. A.; McDonald, T. M.; Bloch, E. D.; Herm, Z. R.; Bae, T.-H.; Long, J. R. *Chem. Rev.* **2012**, *112*, 724.

(2) Kim, J.; Chen, B.; Reineke, T. M.; Li, H.; Eddaoudi, M.; Moler, D. B.; O'Keeffe, M.; Yaghi, O. M. *J. Am. Chem. Soc.* **2001**, *123*, 8239.

(3) Furukawa, H.; Ko, N.; Go, Y. B.; Aratani, N.; Choi, S. B.; Choi, E.; Yazaydin, A. O.; Snurr, R. Q.; O'Keeffe, M.; Kim, J.; Yaghi, O. M. *Science* **2010**, *329*, 424.

(4) Farha, O. K.; Yazaydin, A. O.; Eryazici, I.; Malliakas, C. D.; Hauser, B. G.; Kanatzidis, M. G.; Nguyen, S. T.; Snurr, R. Q.; Hupp, J. T. *Nat. Chem.* **2010**, *2*, 944.

(5) Farha, O. K.; Eryazici, I.; Jeong, N. C.; Hauser, B. G.; Wilmer, C. E.; Sarjeant, A. A.; Snurr, R. Q.; Nguyen, S. T.; Yazaydin, A. O.; Hupp, J. T. *J. Am. Chem. Soc.* **2012**, *134*, 15016.

(6) Grunker, R.; Bon, V.; Muller, P.; Stoeck, U.; Krause, S.; Mueller, U.; Senkovska, I.; Kaskel, S. *Chem. Commun.* **2014**, *50*, 3450.

(7) Wang, T. C.; Bury, W.; Gomez-Gualdron, D. A.; Vermeulen, N. A.; Mondloch, J. E.; Deria, P.; Zhang, K.; Moghadam, P. Z.; Sarjeant, A. A.; Snurr, R. Q.; Stoddart, J. F.; Hupp, J. T.; Farha, O. K. *J. Am. Chem. Soc.* **2015**, *137*, 3585.

(8) Li, J.-R.; Ma, Y.; McCarthy, M. C.; Sculley, J.; Yu, J.; Jeong, H.-K.; Balbuena, P. B.; Zhou, H.-C. *Coord. Chem. Rev.* **2011**, *255*, 1791.

(9) Keskin, S.; van Heest, T. M.; Sholl, D. D. *ChemSusChem* **2010**, *3*, 879.

(10) Wang, C.; Xie, Z.; deKrafft, K. E.; Lin, W. *J. Am. Chem. Soc.* **2011**, *133*, 13445.

(11) Fu, Y.; Sun, D.; Chen, Y.; Huang, R.; Ding, Z.; Fu, X.; Li, Z. *Angew. Chem., Int. Ed.* **2012**, *51*, 3364.

(12) Sun, D.; Fu, Y.; Liu, W.; Ye, L.; Wang, D.; Yang, L.; Fu, X.; Li, Z. *Chem. - Eur. J.* **2013**, *19*, 14279.

(13) Wang, S.; Yao, W.; Lin, J.; Ding, Z.; Wang, X. *Angew. Chem., Int. Ed.* **2014**, *53*, 1034.

(14) Salles, F.; Jobic, H.; Devic, T.; Llewellyn, P. L.; Serre, C.; Ferey, G.; Maurin, G. *ACS Nano* **2010**, *4*, 143.

(15) Sabouni, R.; Kazemian, H.; Rohani, S. *Microporous Mesoporous Mater.* **2013**, *175*, 85.

(16) Saha, D.; Bao, Z.; Jia, F.; Deng, S. *Environ. Sci. Technol.* **2010**, *44*, 1820.

(17) Zhao, Z.; Li, Z.; Lin, Y. S. *Ind. Eng. Chem. Res.* **2009**, *48*, 10015.

(18) Heinke, L.; Gu, Z.; Woll, C. *Nat. Commun.* **2014**, *5*, 4562.

(19) Fletcher, A. J.; Cussen, E. J.; Prior, T. J.; Rosseinsky, M. J.; Kepert, C. J.; Thomas, K. M. *J. Am. Chem. Soc.* **2001**, *123*, 10001.

(20) Hu, X.; Brandani, S.; Benin, A. I.; Willis, R. R. *Ind. Eng. Chem. Res.* **2015**, *54*, 5777.

(21) Liu, J.; Wang, Y.; Benin, A. I.; Jakubczak, P.; Willis, R. R.; LeVan, M. D. *Langmuir* **2010**, *26*, 14301.

(22) Sun, M. S.; Talu, O.; Shah, D. B. *AIChE J.* **1996**, *42*, 3001.

(23) Yazaydin, A. O.; Benin, A. I.; Faheem, S. A.; Jakubczak, P.; Low, J. J.; Willis, R. R.; Snurr, R. Q. *Chem. Mater.* **2009**, *21*, 1425.

(24) Yang, Q.; Zhong, C. *J. Phys. Chem. B* **2006**, *110*, 17776.

(25) Liu, B.; Smit, B. *Langmuir* **2009**, *25*, 5918.

(26) Yang, Q.; Xue, C.; Zhong, C.; Chen, J.-F. *AIChE J.* **2007**, *53*, 2832.

(27) Chui, S. S.-Y.; Lo, S. M.-F.; Charmant, J. P. H.; Orpen, A. G.; Williams, I. D. *Science* **1999**, *283*, 1148.

(28) Chowdhury, P.; Bikkina, C.; Meister, D.; Dreisbach, F.; Gumma, S. *Microporous Mesoporous Mater.* **2009**, *117*, 406.

(29) Liang, Z.; Marshall, M.; Chaffee, A. L. *Energy Fuels* **2009**, *23*, 2785.

(30) Li, L.; Sun, F.; Jia, J.; Borjigin, T.; Zhu, G. *CrystEngComm* **2013**, *15*, 4094.

(31) Wang, Y.; LeVan, M. D. *Ind. Eng. Chem. Res.* **2008**, *47*, 3121.

(32) Glover, T. G.; Wang, Y.; LeVan, M. D. *Langmuir* **2008**, *24*, 13406.

(33) Wang, Y.; Mahle, J. J.; Furtado, A. M. B.; Glover, T. G.; Buchanan, J. H.; Peterson, G. W.; LeVan, M. D. *Langmuir* **2013**, *29*, 2935.

(34) Grajciar, L.; Wiersum, A. D.; Llewellyn, P. L.; Chang, J.-S.; Nachtigall, P. *J. Phys. Chem. C* **2011**, *115*, 17925.

(35) Wang, Q. M.; Shen, D.; Bulow, M.; Lau, M. L.; Deng, S.; Fitch, F. R.; Lemcoff, N. O.; Semanscin, J. *Microporous Mesoporous Mater.* **2002**, *55*, 217.

DOI: 10.1021/jacs.6b05930
J. Am. Chem. Soc. 2016, 138, 11449−11452